J. Fluid Mech. (2004), *vol.* 499, *pp.* 327–343.
DOI: 10.1017/S0022112003006980 Printed in the United Kingdom

The interaction of the piston vortex with a piston-generated vortex ring

By JOHN E. CATER[1], JULIO SORIA[1] AND T. T. LIM[2]

[1]Laboratory for Turbulence Research in Aerospace & Combustion, Department of Mechanical Engineering, Monash University, P.O. Box 31, Melbourne, Victoria 3800, Australia

[2]Mechanical Engineering Department, National University of Singapore, 10 Kent Ridge Crescent, Singapore 119260, Singapore

(Received 10 April 2001 and in revised form 25 July 2003)

This paper presents the results of an experimental investigation of the effects of a piston vortex on the vorticity evolution of a vortex ring. The rings are produced by the roll-up of a shear layer at a circular orifice in a plane wall and have a Reynolds number of 2000 based on the ejection velocity and orifice diameter. The generation mechanism is a piston moving inside a cylinder with a stroke length of two piston diameters. The experimental apparatus is similar to that used by Glezer & Coles (1990) where the piston finishes flush with the orifice, with the result that a piston vortex produced by the apparatus interacts with the vortex ring. Instantaneous velocity field measurements using cross-correlation digital particle image velocimetry reveal that the piston vortex not only increases the circulation of the ring but also creates an asymmetric vorticity distribution of the vortex core. It is found that 'imperfect' merging of the piston vortex with the primary vortex ring promotes the growth of an instability which leads to early transition to turbulence of initially laminar vortex rings.

1. Introduction

The term vortex ring refers to a bounded region of vorticity in a fluid in which vortex lines form closed loops. The bounded region is usually referred to as the core of the ring. The vortex ring has fascinated researchers for a long time, partly due to its intrinsic properties, and partly due to its possible technological applications. The compact nature of a vortex ring also makes it ideal as a simple building block in modelling more complex flows such as the round jets described in Verzicco *et al.* (1997). A great deal of research has been conducted in this area over the past couple of decades, and a review of this work can be found in Shariff & Leonard (1992), and Lim & Nickels (1995).

In most laboratory studies, a vortex ring is produced by moving a piston through a cylindrical tube with an open end protruding into a body of fluid. The resulting cylindrical vortex sheet, which forms at the tube exit, immediately rolls up into a vortex ring (henceforth referred to as the primary ring). However, as soon as the piston stops at the end of the generation process, a secondary vortex ring of opposite circulation is formed on the external surface of the tube exit. The secondary ring is found to affect not only the size, but also the stability of the primary ring. In an attempt to eliminate the secondary flow, Glezer & Coles (1990) designed a generator based on the setup shown in figure 1. It operates in such a way that at the beginning

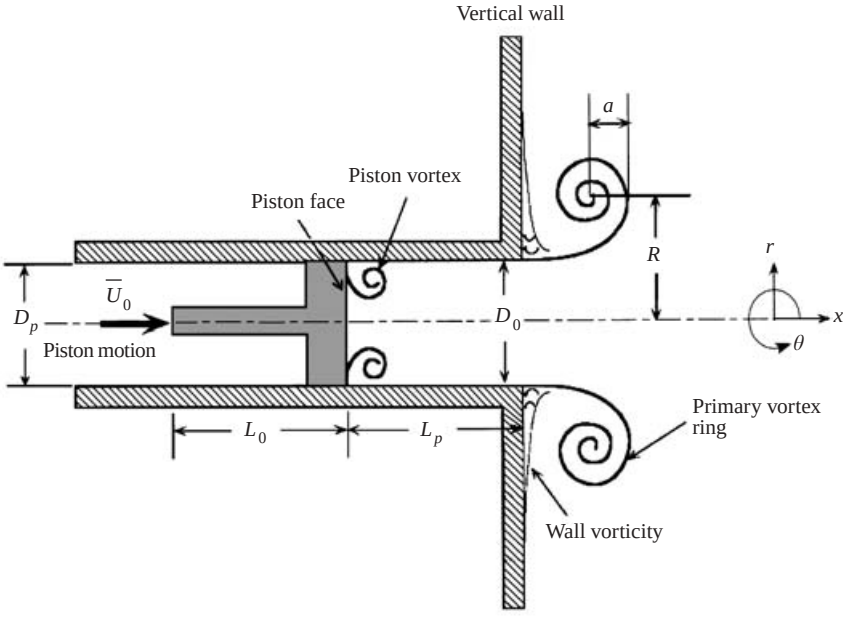

FIGURE 1. Geometric parameters of a piston/cylinder vortex ring generator. D_p is the piston diameter and D_0 is the orifice diameter. In this study $D_0 = D_p = 50$ mm. The mean piston velocity (or 'slug-flow velocity') is $\overline{U_0}$ and L_0 is the stroke length of the piston. L_p is the distance from the lip of the orifice to the piston face at the end of the piston stroke. For the vortex ring, R is the major radius of the toroidal vortex rings and a is an estimate of the radius of the core. Shaded areas indicate solid surfaces. Flow is from left to right.

of the generation process, the geometrical configuration is a simple cylindrical cavity in a plane wall, and at the end of the generation process the wall becomes an uninterrupted plane as the front face of the piston is flush with the wall. This is in contrast to most of the previous studies in which the piston ends well away from the tube exit at the end of the run.

Although Glezer & Coles succeeded in reducing the initial overshoot in the flux of vorticity into the ring, and minimizing the flux vorticity of opposite sign from the wall boundary layer, they also inadvertently introduced a piston vortex into the flow as observed and first measured by Cater, Soria & Lim (1998*a*). This vortex is produced at the piston face as it scrapes the boundary layer from the inside of the cylinder. While inside the cylinder, the influence of the piston vortex on the development of the primary ring is not significant. However, Cater *et al.* (1998*a*) found that as soon as it is ejected into the flow, it is able to interact with the primary ring under certain circumstances. Unlike the secondary vortex ring discussed earlier, these studies found that the piston vortex has the same sign as the primary vortex ring. This is significant as a flow visualization study by Lim (1997*b*) found that the interaction of vortex rings of the same sign (not necessary the same magnitude of circulation) can lead to leap-frogging and eventual merging of all the rings into one. Lim (1997*b*) also observed that the leap-frogging and pairing can enhance transition of an initially laminar primary ring to a turbulent ring; unfortunately, he did not carry out any quantitative measurements.

Based on the observations of Lim (1997*b*), it is reasonable to expect that the piston vortex will also interact with the primary ring in a similar manner, but exactly how

the piston vortex affects the primary ring remains unclear. Allen, Auvity & Smits (2000) examined the initial trajectory of the ring core, which was reported with a large scatter at axial distances greater than one diameter from the orifice, but they did not address the more important question of how the piston vortex affects the vorticity distribution at the core of the primary ring. Preliminary results addressing this question were reported at the 1998 7th European Turbulence Conference by Cater *et al.* (1998*a*) and the work presented in this article is a continuation of that, where this question is addressed in more detail.

2. Experimental technique

2.1. *Experimental apparatus*

The experiments were performed in an acrylic tank, 1000 mm long, 500 mm wide and 500 mm deep, filled with filtered water. Figure 1 shows a schematic drawing of the vortex ring generator used in the present investigation. The fluid was at rest before the start of each experiment, and the vortex rings were produced by ejecting water from a circular cylinder of inner diameter $D_p = 50$ mm into quiescent fluid using a piston. The piston is driven by a computer-controlled stepper motor with a resolution of 25000 steps per rev and a pitch of 5 mm per rev. The maximum acceleration of the motor of 1.0 rev s^{-2} was used throughout this study. Note that the tube exit is flush with the inside surface of one of the endwalls of the tank. The x-axis is measured in the streamwise direction from the centre of a plane containing the tube exit and it coincides with the axis of symmetry of the rings; r is the radial coordinate measured from the x-axis and θ is the azimuthal direction. L_p refers to the distance of the front face of the piston from the tube exit at the end of the piston motion. Therefore, when $L_p = 0$, the front face of the piston is flush with the sidewall and the configuration is identical to that used by Glezer & Coles (1990). Accordingly, this configuration is referred to as the 'piston flush geometry'. In the present investigations, two L_p values are considered, $L_p = 2D_0$ and the piston flush geometry ($L_p = 0$) where D_0 is the orifice diameter.

In a recent investigation of the formation process of vortex rings, Gharib, Rambod & Shariff (1998) found that if the ratio of the piston stroke length to the orifice diameter $L_D = L_0/D_0$ is greater than about 4.0 and the Reynolds number is between 850 and 5000, the leading-edge vortex ring is accompanied by a trailing jet. To prevent this from occurring, $L_D = 2$ was used throughout the present study.

A single value of $Re_{U_0} = 2000$ was selected for the purposes of this investigation, but small variations in the Reynolds number ($< 3\%$) were observed during the course of this study because of slight changes in viscosity due to temperature variation. The above Reynolds number is based on the mean piston velocity of $\overline{U_0} = 0.04$ m s^{-1}. In terms of the circulation based on the slug flow model, the Reynolds number is approximately $Re_\Gamma = 2100$. However, it is not meaningful in this investigation to base the Reynolds number on the initial circulation of the vortex ring because of the contamination of the primary ring by the piston vortex when $L_p = 0$.

2.2. *Velocity measurement technique*

A particle image velocimetry (PIV) technique is used throughout this investigation to measure the velocity fields. This technique is ideal for resolving the in-plane velocity fields without intrusion into the flow. To perform PIV the flow was seeded with nylon spheroids of nominal diameter 28 μm with a specific gravity of 1.03. The particles were illuminated by two co-planar pulsed laser sheets generated by twin Nd:YAG

lasers. These lasers have a pulse width of 6 ns and a temporal pulse separation of $\Delta t = 34$ ms. The lasers were combined along a single optical path and the beams were collimated in one direction to 1.6 mm before being spread into a laser sheet in the orthogonal direction by a cylindrical lens. The sheet provides the illumination of the particles on an (x, r)-plane and has a width of 300 mm at the orifice. The digital image acquisition was performed using a PCO SensiCam digital camera with a 1280×1024 pixels^2 CCD array. Timing of the lasers and the digital camera was controlled to an accuracy of 8 μs using a Pentium based PC.

The data collected were analysed using a multigrid cross-correlation analysis as described in Soria, Cater & Kostas (1999) using a sampling window size of 32×32 pixels^2, and a separation between samples of $\Delta = 0.039 D_0$. This results in a vector grid of 77×61 vectors across the imaged domain. To investigate changes in the vortex ring structure with axial distance, 12 separate camera positions were used at sequential spacings of $1D_0$ from the orifice and the interrogated region at each camera position measured $3.1D_0 \times 2.5D_0$. At each camera location 64 independent velocity vector field measurements were obtained. Note that each of the 64 measurements was taken at the same instant relative to the end of the piston motion.

A second and more detailed study of the formation of the vortex rings was conducted at higher spatial resolution. In this study, the interrogated region at each camera position measured $1.4D_0 \times 1.4D_0$ with a velocity sample separation of $\Delta = 0.022 D_0$. To maximize the spatial resolution of the velocity measurements of the vortex core region in the second study, measurements were only made of one half of the vortex ring. The symmetry of the ring about the horizontal axis at $t = 1.12T_0$ was verified by comparing 128 measurements of both the top and the bottom half of the ring, and no significant difference was found between the position, size or velocity profile of rings in either half, although marked differences were visible at positions further downstream.

2.2.1. *Determination of vorticity evolution*

In this article, the evolution of the vorticity is examined using the vorticity evolution equation for an incompressible fluid with homogeneous properties:

$$\frac{\partial \omega_i}{\partial t} = -u_j \frac{\partial \omega_i}{\partial x_j} + \omega_j s_{ij} + \nu \frac{\partial^2 \omega_i}{\partial x_j \partial x_j}. \tag{2.1}$$

It is derived by taking the curl of the velocity evolution equations. The right-hand side of (2.1) is the summation of three distinct parts. The first term describes the convective transport of a fluid element with vorticity by the velocity field. The second part represents the amplification and rotation of the vorticity vector by the rate-of-strain field, denoted by the symmetric part of the velocity gradient tensor, s_{ij}. The final part represents the diffusion of vorticity throughout the fluid by viscosity.

The present study is restricted to axisymmetric vortex rings generated at a circular opening without the presence of a mean swirl velocity (u_θ). For a laminar axisymmetric vortex ring the only non-zero component of vorticity is the azimuthal component. In this study, PIV velocity fields obtained at each measurement location were used to calculate the out-of-plane vorticity field (ω_θ) using a thirteen-point least-squares fit to the velocity field, followed by analytic differentiation based on

$$\omega_\theta = \frac{\partial u_r}{\partial x} - \frac{\partial u_x}{\partial r}. \tag{2.2}$$

This vorticity was non-dimensionalized by the orifice diameter and twice the mean orifice velocity ($D_0/2\overline{U_0}$). At each measurement instant, the location of the peak vorticity was found using a linear search and a local two-dimensional Gaussian least-squares fit was used to determine the magnitude of the peak vorticity and its location more precisely. The location of the peak is given by the coordinates (x_c, r_c). The assumption that the core has a Gaussian distribution is examined later in this article.

The stretching of azimuthal vorticity is determined by the out-of-plane rate-of-strain components:

$$\frac{1}{2}\left(\frac{\partial u_\theta}{\partial x}+\frac{1}{r}\frac{\partial u_x}{\partial \theta}\right), \frac{1}{2}\left(\frac{\partial u_\theta}{\partial r}+\frac{1}{r}\frac{\partial u_r}{\partial \theta}\right), \frac{1}{r}\frac{\partial u_\theta}{\partial \theta}.$$

Of these, only the rate of change in the out-of-plane component of velocity $(1/r)(\partial u_\theta/\partial\theta)$ can be determined from two-dimensional measurements. This quantity is the azimuthal rate-of-strain component which can be calculated by invoking the continuity relationship in cylindrical coordinates

$$\frac{\partial u_x}{\partial x}+\frac{\partial u_r}{\partial r}+\frac{1}{r}\frac{\partial u_\theta}{\partial \theta}=0. \tag{2.3}$$

The unknown quantity $(1/r)(\partial u_\theta/\partial\theta)$, is calculated by the addition of the other two velocity gradients.

2.3. *Error estimation*

The accuracy of the vorticity field measurements depends not only on the spatial sampling distance between the velocity data points, but also on the accuracy of the velocity vector field measurements. These two factors depend on the velocity measurement technique used. With PIV, the accuracy is affected by the spatial resolution of the recording medium, the ratio of seed particle diameter to the vorticity distribution length scale and the seeding density of the particles. In addition, the accuracy of the ω_θ measurement is dependent on the computational method used to analyse the measured in-plane velocity vector field data. In this regard, the method of Fouras & Soria (1998) was utilized to estimate the errors introduced by the thirteen-point least-squares-fit calculations used in the analysis. At $t=1.12T_0$ the under-estimation of the peak vorticity due to bias error is 9% and the random error in the peak measurement is 8% at the 95% confidence level. The magnitude of the bias error decreases with increasing vortex ring core size.

2.4. *Factors influencing vortex propagation*

Owing to the confined nature of the tank, which measures $20D_0 \times 10D_0 \times 10D_0$, the distance to which the evolution of the vortex rings can be followed is somewhat restricted. A previous study by Walker *et al.* (1987) found that when a vortex ring is in the vicinity of the wall, its propagation velocity decreases. To limit the influence of the endwall on the ring revolution, the present investigation has been limited to regions within the first half of the tank, up to a distance of $10D_0$.

Also, when a series of rings is generated, it is likely that the trajectory of one ring may be influenced by the velocity field of the previous vortex ring if the time interval between them is too short. Based on our extensive studies, it was found that a 4 minute time interval is necessary in order to avoid measurable change in the position or standard deviation of the position of the peak vorticity from ring to ring. Note that to minimize the random error due to sample size of the above statistical data, several hundred ring realizations were used in the analysis. As an extra precaution, all the vortex rings examined in this work were generated at least 8 minutes apart.

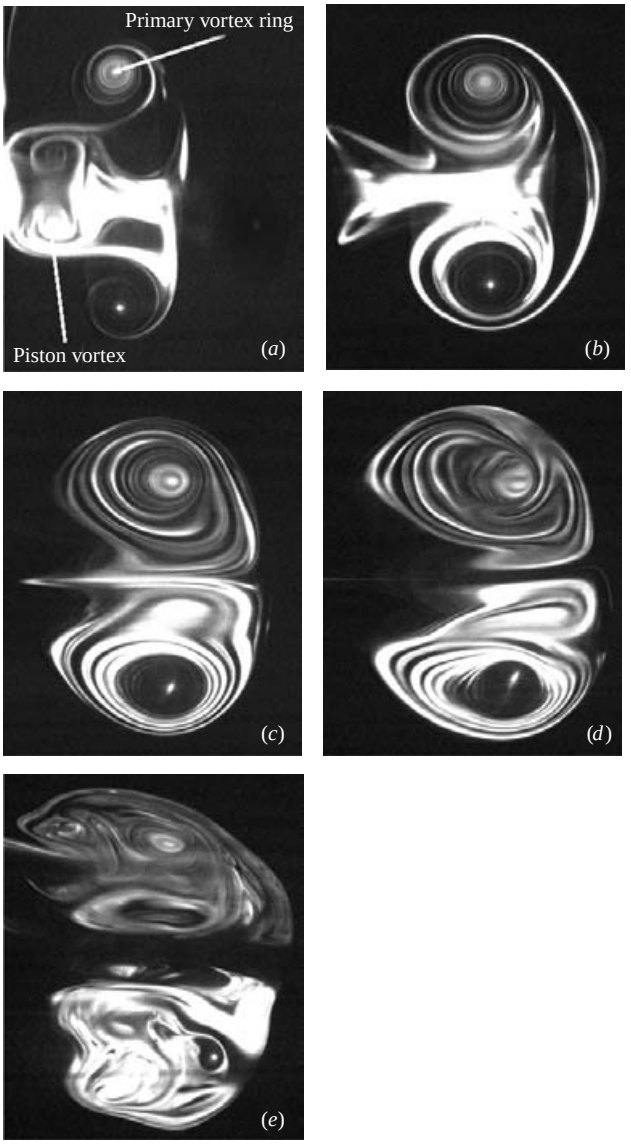

FIGURE 2. A sequence of digital images showing the interaction of the piston vortex with a primary vortex ring when $L_p = 0$. The interaction causes the piston vortex to slip through the primary ring and eventually merge with it. The imperfect merging causes the early transition to turbulence of the initially laminar ring.

3. Results and discussion

3.1. *Initial ring circulation and core size*

An initial flow visualization study using Kiton Red 620 fluorescent dye revealed qualitatively the influence of the piston vortex on the evolution of the primary ring. Figure 2 shows a sequence of images of the vortex ring acquired at axial locations spaced $2D_0$ apart when $L_p = 0$. The first image shows the piston vortex within the primary ring and the following images show the merging of the primary ring and the piston vortex and the transition to turbulence of the combined ring. In contrast

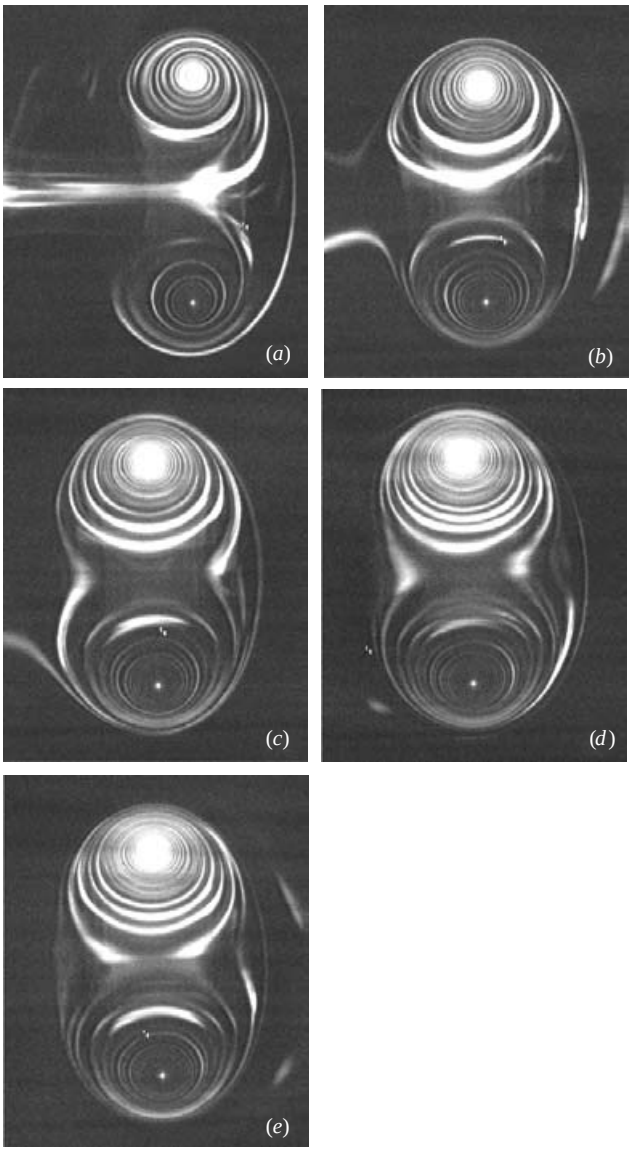

FIGURE 3. A sequence of digital images showing the generation of the primary vortex ring when $L_p = 2D_0$. In this case, the piston vortex is confined within the tube. The resulting vortex ring appears to translate steadily up to an axial displacement of $x = 10D_0$.

figure 3 shows the evolution of the primary ring when the piston vortex does not emerge. In this case, the primary vortex ring remains laminar throughout the observed domain. These images are acquired at the same instant as those shown in figure 2.

The circulation of the vortex ring is calculated from the PIV velocity field using a square circuit around the peak vorticity location where the core is, with one edge along the centreline of the ring. The measured circulation was monitored as a function of time to establish its maximum value. It is found that the maximum circulation coincides with the time at which the rings 'pinch-off' and the fluid surrounding the core begins to propagate downstream. At this point in time, which is found to be

	Γ_0/Γ_{slug}	a_0/D_0	Remarks
Pullin (1979) Similarity Model	0.888	–	Tube geometry
Didden (1979) (LDA)	1.300	–	Tube geometry with trapezoidal profile
Glezer (1988) Slug Model	1.011	0.5	Piston in cavity
Weigand & Gharib (1997) (PIV)	0.995	–	Tube geometry, different velocity profile
$L_p = 2D_0$ (present result)	1.228	0.135	The piston finishes $2D_0$ from tube exit
$L_p = 0$ (present result)	1.396	0.145	The piston face finishes flush

TABLE 1. Initial ring circulation.

approximately $2.2T_0$ for both geometries, all the vorticity has been ingested so that the circulation value represents the total circulation of the vortex ring.

Table 1 shows the measured circulation and core size of the rings obtained in this investigation. For completeness, the similarity model of Pullin (1979), and the experimental results of Didden (1979), Glezer (1988) and Weigand & Gharib (1997) are also included. The circulation is non-dimensionalized by the circulation obtained using the slug-flow model:

$$\Gamma_{slug} = \tfrac{1}{2} P \overline{U_0} L_0, \tag{3.1}$$

where L_0 is the distance moved by the piston and $\overline{U_0}$ is the mean velocity of the piston. P is a velocity program factor that takes into account the acceleration period of the slug, and is defined by

$$P = \int_0^1 \left(\frac{U_0^2}{\overline{U_0^2}} \right) \mathrm{d}\left(\frac{t}{T_0} \right) = \frac{\overline{U_0^2}}{\overline{U_0^2}}, \tag{3.2}$$

where t represents the acceleration time and T_0 the total duration of the piston motion. In this particular study, P is found to be 1.01 which corresponds to a trapezoidal velocity profile.

These results show that when the piston finishes flush, the initial circulation of the region around the vortex ring is 39.6% higher than the slug circulation, while when $L_p = 2D_0$, it is 22.8% above that of the slug model.

Note that it is not possible to make a direct comparison of our results with those tabulated above because the vortex ring generators used differ. As shown in our results, the overall circulation and the core size of the rings depend very much on the manner in which they are generated. For the case where the piston finishes flush with the endwall (i.e. $L_p = 0$), these quantities are distinctly higher than those when $L_p = 2D_0$. This finding shows that the piston vortex has a considerable influence on the overall circulation and vortex core of the resulting ring.

3.2. *Mean vortex ring motion*

In figure 4, the mean translational velocity for 64 realizations of the velocity centroid for both generating conditions is presented. The results show that the vortex ring produced when $L_p = 0$ has consistently greater streamwise velocity than that when $L_p = 2D_0$. This finding is consistent with the increase in the circulation of the vortex ring when $L_p = 0$ (see table 1).

Interestingly, when $t > 8\ T_0$, the vortex ring produced when $L_p = 0$ suddenly undergoes a flow transition, resulting in a steeper decrease in the propagation velocity compared to the case when $L_p = 2D_0$ This rapid deceleration can be attributed to the increase in the entrainment of ambient fluid (see Saffman 1978) as a result of

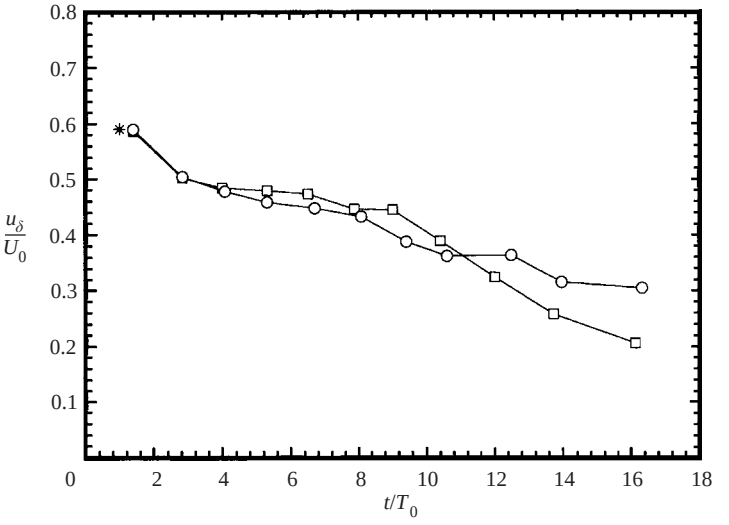

FIGURE 4. Non-dimensional vortex ring axial translation velocity u_δ/U_0, as a function of formation time, $Re_0 = 2000$. The velocity is non-dimensionalized by the slug flow velocity U_0: $L_p = 2D_0$ (○), $L_p = 0$ (□). Also shown is the value of the empirical fit for the initial velocity of a vortex ring by Didden (1979) (∗).

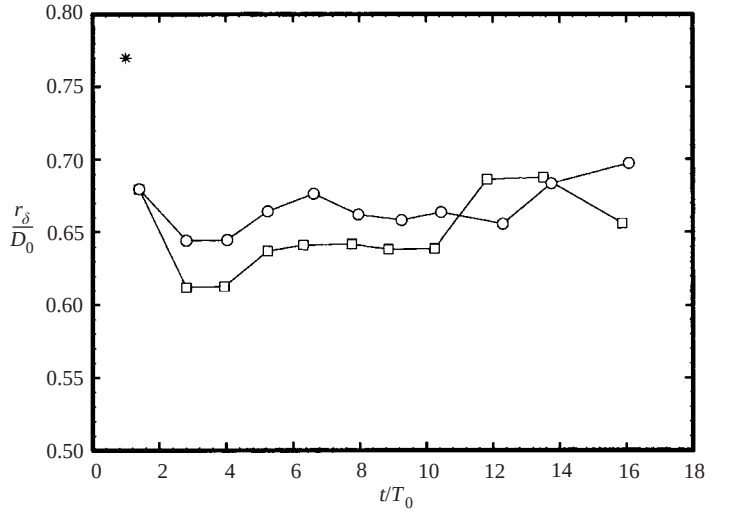

FIGURE 5. Non-dimensional vortex ring core radius r_δ/D_0, for laminar vortex rings with $Re_0 = 2000$, as a function of non-dimensional ring formation time for the different formation geometries: $L_p = 2D_0$ (○), $L_p = 0$ (□). The empirical fit of Didden (1979) is also shown (∗).

the early transition to a turbulent ring. This finding suggests that the piston vortex enhances the transition from a laminar ring to a turbulent ring.

Figure 5 shows the radial position of the peak vorticity location non-dimensionalized by the orifice diameter. The trajectory of the core is noticeably different for $L_p = 2D_0$ and $L_p = 0$. Although both sets of rings contract in diameter initially, the reduction is most marked in the case when $L_P = 0$. This is probably caused by the piston vortex having moved ahead of the primary vortex ring, which

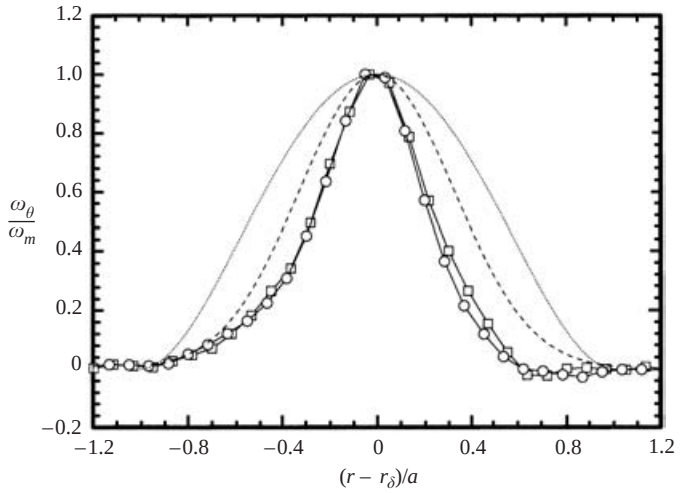

FIGURE 6. Radial profiles of normalized vorticity for vortex rings with $Re_0 = 2000$: $L_p = 2D_0$ (○), $L_p = 0$ (□). The vorticity values are normalized with the peak value measured when the axial coordinate, x_c, of the peak is $2D_0$. The profiles are compared to the polynomial distribution used by Widnall *et al.* (1974), $\omega = (r^2 - 1)^2$ (– –), and a Gaussian fit with $\eta = 4.7$ from Weigand & Gharib (1997), $\omega = \exp(-\eta^2 r^2)$ (· · ·).

induces a velocity field that causes the diameter of the primary ring to contract. After the initial contraction, both rings increase in diameter as they propagate downstream, up to at least $10T_0$. Beyond $10T_0$, the radial position is difficult to determine as the ring has undergone transition and the core region becomes less distinct. Nevertheless, an increase in ring diameter is consistent with a decrease in ring velocity if momentum is considered.

3.3. *Vorticity fields*

Figure 6 shows the normalized vorticity distribution of the vortex core ω_θ for the case where $x_c = 2D_0$. For the purpose of comparison, the existing vortex formation models of Widnall, Bliss & Tsai (1974) and the data of Weigand & Gharib (1997) are also presented. Note that the result of Weigand & Gharib (1997) has been curve fitted with a Gaussian best fit. It can be seen that our results agree reasonably well with the experimental result of Weigand & Gharib (1997), and that the experimentally determined core size is smaller than that predicted by the theoretical model. The present study also indicates that the profiles of vorticity can be approximated by a Gaussian distribution. This finding supports the numerical study of Shariff, Verzicco & Orlandi (1994) which used Gaussian initial conditions.

Figure 7 shows the corresponding normalized profiles of ω_θ in the axial direction at $x_c = 2D_0$. Note that the distribution of azimuthal vorticity in this direction is considerably wider and consequently fewer data were obtainable within the fixed imaged region. It can be seen that there is also a distinct asymmetry between the front (positive $(x - x_c)/a$) and the rear of the ring. The tendency for the rear of the ring to elongate is consistent with the strain induced by curvature.

The evolution of the vorticity distribution for the condition $L_p = 2D_0$ is shown in figure 8. Each field is calculated for a vortex ring with the ratio of the piston stroke length to the orifice diameter of $L_D = 2.0$. As presented, the orifice is located at $x = 0$ and the centreline for the ring is at $r = 0$. Successive frames show how the vorticity

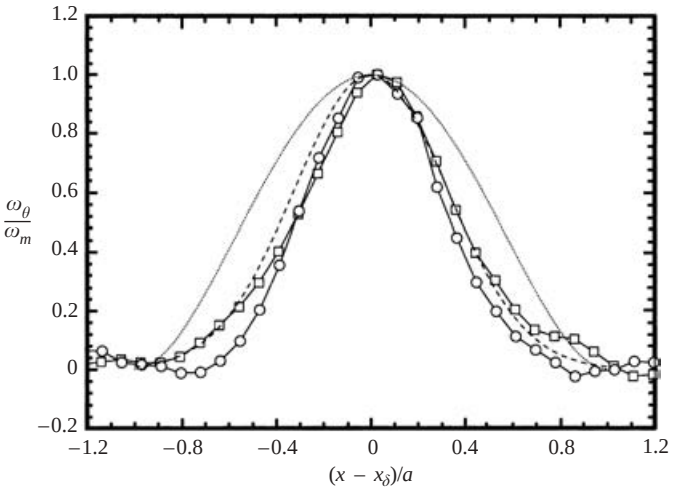

FIGURE 7. As figure 6 but showing axial profiles.

field evolves with time and distance from the generator. The vorticity evolution for the case when $L_p = 0$ is shown in figure 9.

These results show that the out-of-plane vorticity distribution at the core of the primary vortex ring is initially circular in shape and has roughly the same size for both $L_p = 2D_0$ and $L_p = 0$. The results also show that the measured vorticity distributions at generation are sharply peaked, which agrees with the suggestion by Saffman (1978). However, as soon as the vortex core is separated from the nozzle, it elongates in the direction of the ring propagation into an ellipse due to the self-induced strain field. This occurs between the distributions shown in figures 8(*a*) and 8(*b*), and figures 9(*a*) and 9(*b*). The elliptical distribution has also been noted in the dye visualizations of Maxworthy (1972).

As the vortex ring with $L_p = 0$ propagates, an angle of tilt appears to develop between the major axis of the ellipse and the axis of symmetry of the ring in the measured plane. This behaviour is an artifact of a wavy azimuthal distribution in the axial plane as reported by Cater (2002). The orientation of the major axis of the core is thus a function of θ. Flow visualization indicates that there are five 'kinks' in the azimuthal vortex filament for this Reynolds number and geometry. The odd number of waves explains the differing behaviour of vorticity distributions at the two values of θ shown in the vorticity plots. Other examples of this type of pattern can be seen in Weigand & Gharib (1997) or in the simulations of Shariff *et al.* (1994). The stability of these azimuthal bending waves is examined in Widnall & Sullivan (1973), Widnall *et al.* (1974) and Widnall & Tsai (1977). The breakdown of azimuthal waves is often seen immediately prior to transition.

A recent study by Allen *et al.* (2000) suggests that secondary vorticity may change the initial position and trajectory of the core; however, this is not supported by the present data. Figures 8 and 9 show that the changes in the velocity of the rings become evident only at a much later time in the evolution of the rings, when the piston vortex wraps around the torus of the primary ring core. The remains of the piston vortex are visible in figure 9(*a*) and its merging with the core is visible in figure 9(*a–c*). The work of Allen *et al.* (2000) also suggests that the injection of the piston vortex reduces the diameter of the primary ring as observed here, due to the

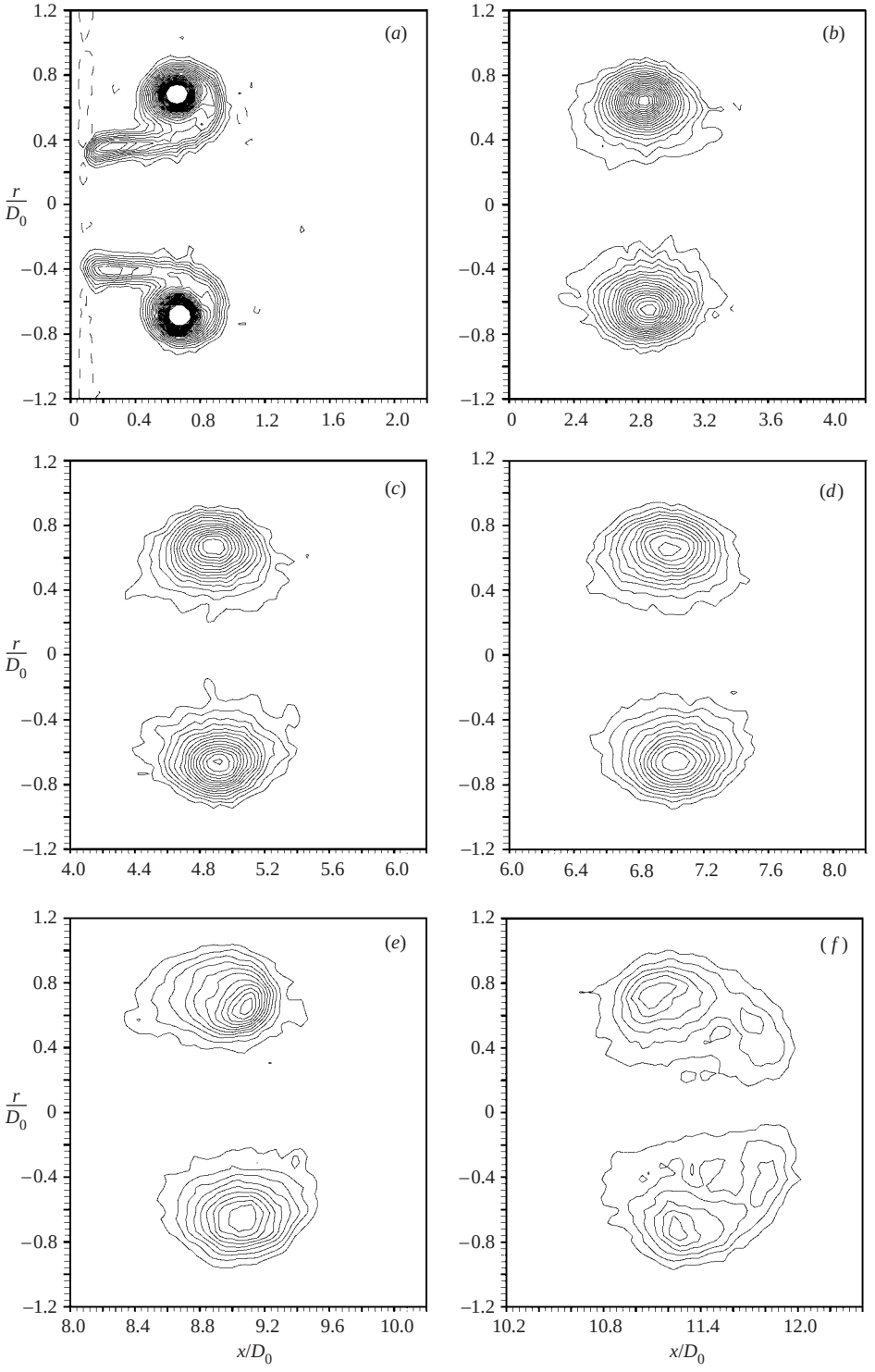

FIGURE 8. Mean azimuthal vorticity $\overline{\omega_\theta} D_0/2\overline{U_0}$, for initially laminar vortex rings and $L_p = 2D_0$ with $Re_0 = 2000$. Contours are at intervals of 0.25. (*a*) $t = 1.4T_0$, (*b*) $t = 4.0T_0$, (*c*) $t = 6.4T_0$, (*d*) $t = 8.9T_0$, (*e*) $t = 11.9T_0$, (*f*) $t = 15.9T_0$.

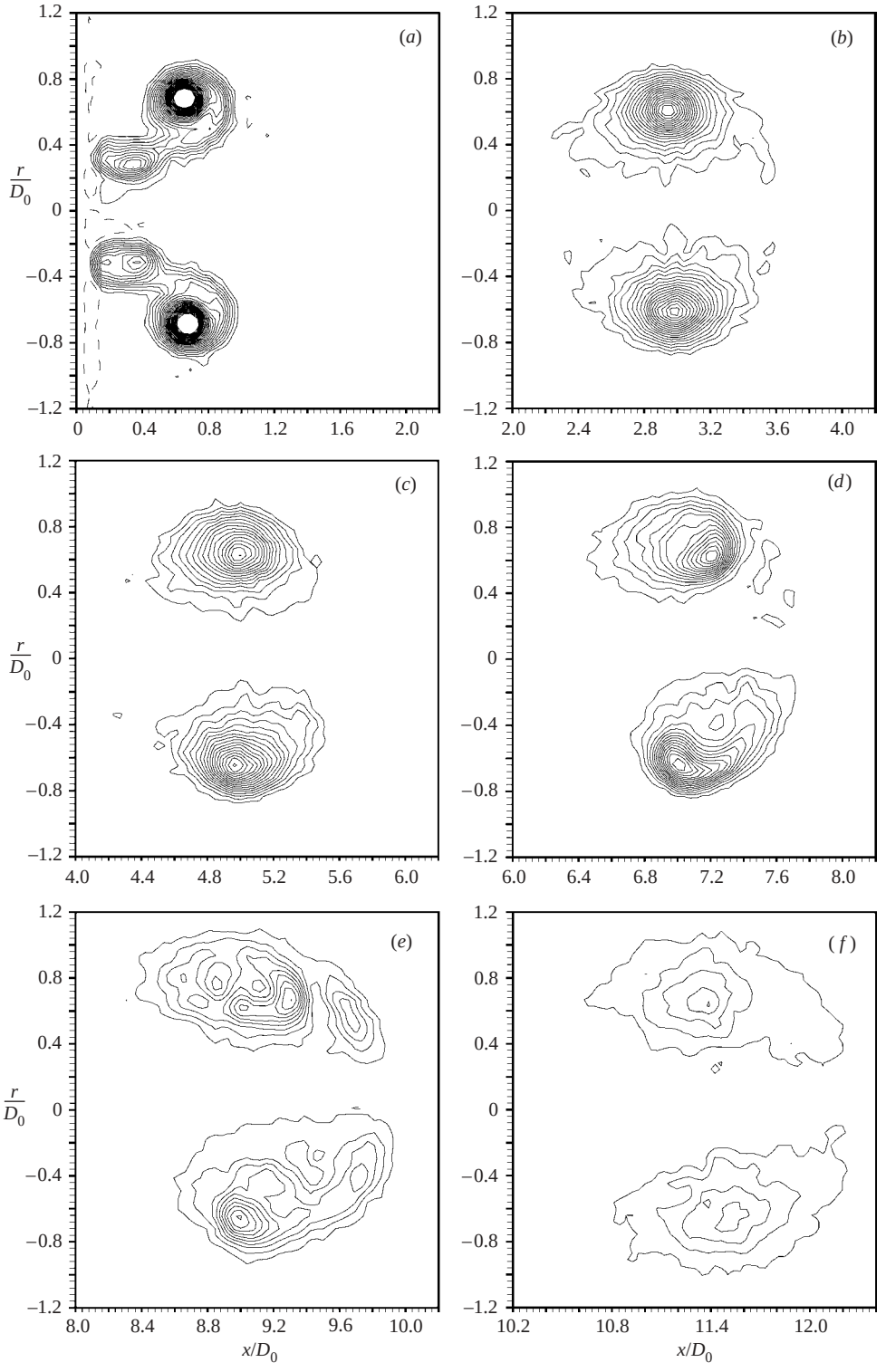

FIGURE 9. As figure 8 but for $L_p = 0$.

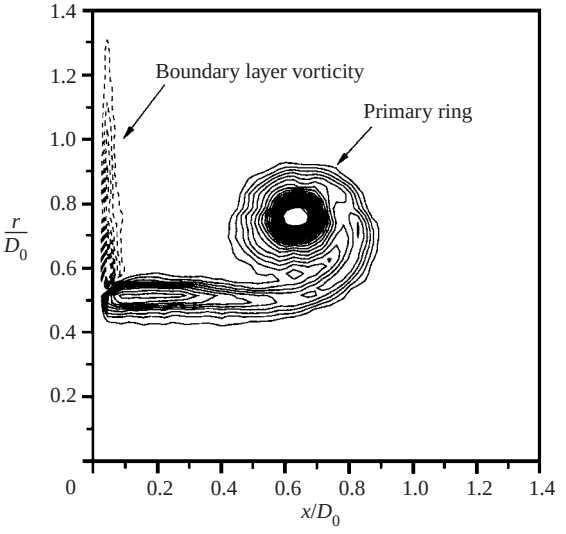

FIGURE 10. Non-dimensionalized azimuthal vorticity $\overline{\omega_\theta} D_0/2\overline{U_0}$, for half of an initially laminar vortex ring. $Re_0 = 2000$, $t = 1.12T_0$. In this case the piston face finishes at $L_p = 2D_0$. Contours are at intervals of 0.5. Dashed lines represent negative vorticity values.

increase in streamwise stretching. Associated with the additional circulation from the piston vortex is a higher velocity at the centre of the vortex ring. This has the effect of causing the forward stagnation point to move downstream.

Figure 10 shows the regions where vorticity is present when the ring is first generated for $L_p = 2D_0$. This figure is similar to figure 8(*a*) except that it has been enlarged to show the detailed vorticity distribution around the tube exit. The primary ring is the large concentration of positive vorticity at the centre of the frame, and there is a thin layer of induced vorticity on the vertical wall on the left-hand side of the figure. The induced vorticity has opposite sense to the primary ring. The regions of intense vorticity are labelled in the figure.

Figure 10 can be contrasted with figure 11 for $L_p = 0$. In this case, the piston vortex is visible as positive vorticity in the lower left-hand corner of the figure. However, below the piston vortex and closer to the ring centreline is vorticity of the opposite sense which has also been generated at the piston face. Allen & Chong (2000) have shown that equal amounts of circulation of both signs are created on the piston face. The circulation for the piston vortex measured in our work at $t = 1.12T_0$ is approximately $0.32\Gamma_0$ which is $0.25\Gamma_{slug}$. This is also in good agreement with the work of Allen *et al.* (2000).

The effects of vorticity from the piston face, such as the piston vortex, can be eliminated by the piston face finishing far from the inside wall or by using an orifice or other flow restriction in front of the piston. The piston vortex is of particular concern at a high value of L_D (i.e. the ratio of the piston stroke length to the orifice diameter), since the strength of the secondary ring will be a function of the piston stroke length. It should also be noted that the effects of vorticity generated at the piston are not restricted to the impulsively started vortex ring flow.

In the present study, the piston vortex visible in figure 11 is of the same sense as the primary ring. It has been shown that secondary vorticity of the same sign can lead to the piston vortex ring leap-frogging the primary ring like the perturbed vortex

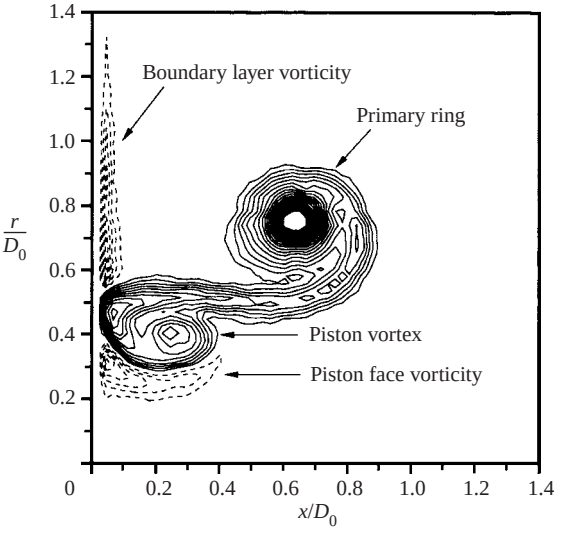

FIGURE 11. As figure 10 but in this case the piston face finishes at $L_p = 0$.

rings described in Lim (1997*a*). In this manner the core of the primary ring becomes distorted, particularly if the leap-frogging is not 'clean' as can be observed in the flow visualization picture in figure 2. This can be compared with figure 3 for the case of $L_P = 2D_0$ where the piston vortex is confined within the tube. It is found that misalignment of the rings during the leap-frogging causes the vortex ring to become unstable and triggers a premature transition to turbulence.

The existence of secondary vorticity outside the ring core that is not part of the piston vortex can also have an influence on the total circulation. Also, there is vorticity of the opposite sign to the primary ring present that is created at the piston face. This can be clearly seen in figure 11. This vorticity appears to be annihilated by some of the vorticity from the piston vortex since it disappears in the next frame and the circulation of the piston vortex is reduced. Similarly, secondary vorticity is induced at the boundary layer on the wall behind the ring during formation. This was observed in both cases. This vorticity has the opposite sign to the primary ring and cancels with the shear layer, which decreases the total circulation. This vorticity is no longer observed after the vortex ring pinches off.

Figure 12 displays the change in the magnitude of the non-dimensional peak vorticity as a function of time. Note that time is non-dimensionalized by the piston stroke period, T_0. The rate of decay can be modelled by the function

$$\frac{\omega_m D_0}{2U_0} = C_0(\nu t)^{-1/2}, \tag{3.3}$$

which is also displayed in the figure. The results show that the peak vorticity initially decays with the viscous timescale while $t \leqslant 8\ T_0$. This time corresponds approximately to the time when the core of the vortex ring generated with $L_p = 0$ deforms into a 'half-moon' shape. The results also show that there is a small increase in peak vorticity at around $t = 8T_0$ when $L_p = 0$ and $t = 12T_0$ when $L_p = 2D_0$. This behaviour could be due to azimuthal stretching of the vortex filaments, which also has the effect of intensifying viscous diffusion of the core. This may explain why there is a greater reduction in the peak vorticity soon after $t = 8T_0$ and $t = 12T_0$.

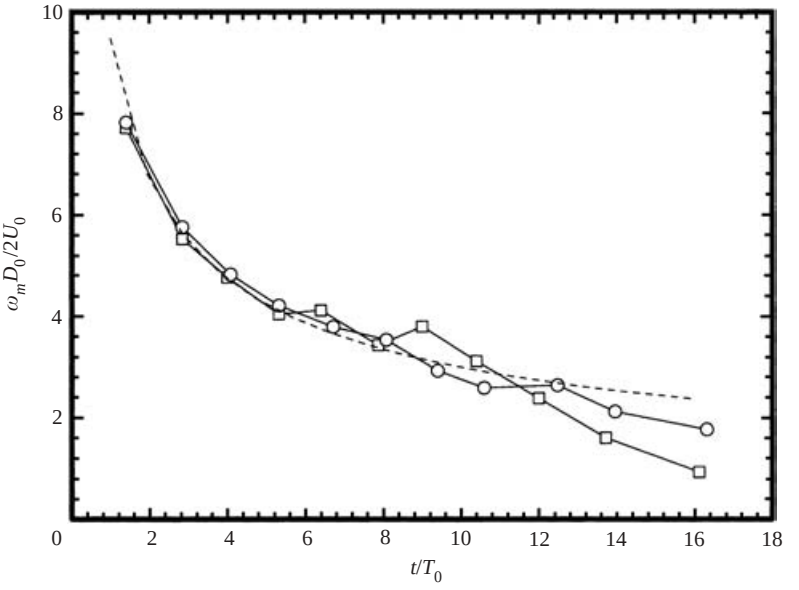

FIGURE 12. Peak non-dimensional azimuthal vorticity for vortex rings as a function of non-dimensional time, $Re_0 = 2000$: $L_p = 2D_0$ (○), $L_p = 0$ (□). The peak vorticity, ω_m, is non-dimensionalized by the orifice diameter and the slug flow velocity. The dashed line shows a curve fit to the data points of the form shown in equation (3.3).

It is important to note that radial perturbations of vorticity will grow when they are aligned with the local principal axis of stretching. In the case of the vortex ring, the ring is most susceptible to instabilities where the axis of stretching is normal to the vorticity contours. This scenario, coupled with the curvature of the vortex ring and the diffusion of vorticity across the ring centreline, will lead to radial asymmetry in coordinates relative to the core. This asymmetry is further amplified in the presence of a piston vortex.

4. Conclusions

This paper has addressed some of the issues concerning the effects of the piston vortex on the primary vortex ring. The results show that when the piston vortex is confined within the tube and far away from the exit, its influence on the primary vortex ring is small. However, when it is ejected into the flow, it interacts with the primary vortex ring, causing changes in the properties of the vortex ring. Not only does it cause the circulation of the primary vortex ring to increase, it also causes a significant modification to the vorticity distribution and evolution of the vortex core. These changes are brought about by an 'imperfect' merging of the piston vortex with the primary vortex ring, which has been shown to also be responsible for a premature transition to turbulence of the initially laminar primary ring.

The financial support by the ARC to undertake this research is gratefully acknowledged.

REFERENCES

ALLEN, J. J., AUVITY, B. & SMITS, A. J. 2000 Interaction of a vortex ring with a piston vortex. In *9th Intl Symp. on Flow Visualization, Edinburgh, UK*.

Allen, J. J. & Chong, M. S. 2000 Vortex formation in front of a piston moving through a cylinder. *J. Fluid Mech.* **416**, 1–28.

Cater, J. E. 2002 An experimental investigation of viscous vortex rings and zero-net-mass-flux jets. PhD thesis, Monash University, Melbourne, Australia.

Cater, J., Soria, J. & Lim, T. T. 1998*a* Vortex ring formation at an orifice. In *Advances in Turbulence VII. Proc. 7th European Turbulence Conf. Saint Jean Cap Ferrat, France* (ed. U. Frisch), *Fluid Mechanics and its Applications*, vol. 46, pp. 11–14. Kluwer.

Cater, J., Soria, J. & Lim, T. T. 1998*b* The vorticity of a vortex ring core. In *13th Australasian Fluid Mechanics Conf. Victoria, Australia* (ed. K. Hourigan & M. C. Thompson). Monash University.

Didden, N. 1979 On the formation of vortex rings: Rolling-up and production of circulation. *Z. Angew Math. Phys.* **30**, 101–116.

Fouras, A. & Soria, J. 1998 Accuracy of out-of-plane vorticity measurements using in-plane velocity vector field data. *Exps. Fluids* **25**, 409–430.

Gharib, M., Rambod, E. & Shariff, K. 1998 A universal time scale for vortex ring formation. *J. Fluid Mech.* **360**, 121–140.

Glezer, A. 1988 The formation of vortex rings. *Phys. Fluids* **31**, 3532–3542.

Glezer, A. & Coles, D. 1990 An experimental study of a turbulent vortex ring. *J. Fluid Mech.* **211**, 243–283.

Lim, T. T. 1997*a* A note on the leapfrogging between two coaxial vortex rings at low Reynolds numbers. *Phys. Fluids* **9**, 239–241.

Lim, T. T. 1997*b* On the role of Kelvin-Helmholtz-like instability in the formation of turbulent vortex rings. *Fluid Dyn. Res.* **21**, 47–56.

Lim, T. T. & Nickels, T. 1995 Vortex rings. In *Fluid Vortices.* Kluwer.

Maxworthy, T. 1972 The structure and stability of vortex rings. *J. Fluid Mech.* **51**, 15–32.

Pullin, D. I. 1979 Vortex ring formation at tube and orifice openings. *Phys. Fluids* **22**, 401–403.

Saffman, P. 1978 The number of waves on unstable vortex rings. *J. Fluid Mech.* **84**, 625–639.

Shariff, K. & Leonard, A. 1992 Vortex rings. *Annu. Rev. Fluid Mech.* **24**, 235–279.

Shariff, K., Verzicco, R. & Orlandi, P. 1994 A numerical study of three-dimensional vortex ring instabilities: Viscous corrections and early non-linear stage. *J. Fluid Mech.* **279**, 351–375.

Soria, J., Cater, J. & Kostas, J. 1999 High resolution multigrid cross-correlation digital PIV measurements of a turbulent starting jet using half frame image shift film recording. *Opt. Las. Technol.* **31**, 3–12.

Verzicco, R., Iafrati, A., Riccardi, G. & Fatica, M. 1997 Analysis of the sound generated by the pairing of two axisymmetric co-rotating vortex rings. *J. Sound Vib.* **200**, 347–358.

Walker, J., Smith, C., Cerra, A. & Doligalski, T. 1987 The impact of a vortex ring on a wall. *J. Fluid Mech.* **181**, 99–140.

Weigand, A. & Gharib, M. 1997 On the evolution of laminar vortex rings. *Exps. Fluids* **22**, 447–457.

Widnall, S. E., Bliss, D. & Tsai, C. 1974 The instability of short waves on a vortex ring. *J. Fluid Mech.* **66**, 35–47.

Widnall, S. E. & Sullivan, J. 1973 On the stability of vortex rings. *Proc. R. Soc. Lond.* A **332**, 335–353.

Widnall, S. E. & Tsai, C. 1977 The instability of a thin vortex ring of constant vorticity. *Proc. R. Soc. Lond.* A **267**, 273–305.